HIV-1 Nef acts in synergy with APOL1-G1 to induce nephrocyte cell death in a new *Drosophila* model of HIV-related kidney diseases

Jun-yi Zhu[1,2], Yulong Fu[1,3], Joyce van de Leemput[1,2] Ying Yu[4], Jinliang Li[5], Patricio E. Ray[4,*], and Zhe Han[1,2,*]

1 Center for Precision Disease Modeling, Department of Medicine, University of Maryland School of Medicine, Baltimore, Maryland

2 Division of Endocrinology, Diabetes and Nutrition, Department of Medicine, University of Maryland School of Medicine, Baltimore, Maryland

3 Current: Department of Pathology, University of Alabama at Birmingham, Birmingham, Alabama

4 Child Health Research Center, Department of Pediatrics, University of Virginia School of Medicine

5 Children's Research Institute, Children's National Hospital, Washington DC

Running title: HIV-1 Nef synergizes with APOL1 in cytotoxicity

Keywords: APOL1, HIV, nephropathy, Nef, nephrocyte, autophagy, HIVAN, *Drosophila*

*** CORRESPONDING AUTHORS**

Dr. Zhe Han, PhD
Center for Precision Disease Modeling
Department of Medicine, University of Maryland School of Medicine
670 West Baltimore Street, Baltimore, MD 21201, USA
Email: zhan@som.umaryland.edu; ORCID identifier: 0000-0002-5177-7798

Dr. Patricio E. Ray MD
Child Health Research Center,
Department of Pediatrics, University of Virginia School of Medicine
Room 2120, MR4 Building, 409 Lane Road, Charlottesville, VA 22908, USA
E-mail: Pray@virginia.edu; ORCID identifier: 0000-0003-2223-9584

HIGHLIGHTS

- Developed a new transgenic *Drosophila* model to study the pathogenesis of HIV-1-related kidney diseases with nephrocyte-specific expression of HIV-1 *nef* and an *APOL1-G1* risk allele derived from a patient with HIVAN.
- APOL1-G1 caused organelle acidification defects, reduced formation of autophagolysosomes, and reduced autophagy and protein aggregation, which culminated in ER stress.
- HIV-1 Nef induced ER stress through an autophagy-independent pathway. In addition, Nef acted through an autophagy-dependent pathway that heightened the ER stress. It did so through APOL1-G1-mediated autophagy pathway disruption, which resulted in nephrocyte dysfunction and cell death.

SIGNIFICANCE STATEMENT

APOL1 risk alleles are strongly linked to HIV-associated nephropathy (HIVAN) in people of African descent, but how HIV-1 and APOL1 interact and which pathways they might converge upon is unclear. A new *Drosophila* model to study HIV-1 Nef and APOL1-G1 (a risk allele) showed that Nef can induce ER stress in nephrocytes by itself, as well as exacerbate the organelle acidification defects and reduced autophagy induced by APOL1-G1, which further stimulates ER stress to a level that could cause nephrocyte cell death. Thus, we identified ER stress as the converging point for the synergy between APOL1-G1 and HIV-1 Nef in kidney cells, providing a potential therapeutic target for HIV-1 and APOL1-associated nephropathies.

ABSTRACT

Background: People carrying two *APOL1* risk alleles (RA) *G1* or *G2* are at greater risk of developing HIV-associated nephropathy (HIVAN). Studies in transgenic mice showed that the expression of HIV-1 genes in podocytes, and *nef* in particular, led to HIVAN. However, it remains unclear whether APOL1-RA and HIV-1 Nef interact to induce podocyte cell death.

Method: We generated transgenic (Tg) flies that express *APOL1-G1* (derived from a child with HIVAN) and HIV-1 *nef* specifically in the nephrocytes, the fly equivalent of mammalian podocytes, and assessed their individual and combined effects on the nephrocyte filtration structure and function.

Results: We found that HIV-1 Nef acts in synergy with APOL1-G1 resulting in nephrocyte structural and functional defects. Specifically, HIV-1 Nef itself can induce endoplasmic reticulum (ER) stress (without affecting autophagy). Through a different pathway, Nef exacerbates the organelle acidification defects and reduced autophagy induced by APOL1-G1. The synergy between HIV-1 Nef and APOL1-G1 is built on their joint effects on elevating ER stress, triggering nephrocyte dysfunction and ultimately cell death.

Conclusions: A new *Drosophila* model of HIV-1-related kidney diseases identified ER stress as the converging point for the synergy between HIV-1 Nef and APOL1-G1 in inducing nephrocyte cell death. Given the high relevance between *Drosophila* nephrocytes and human podocytes, this finding suggests ER stress as a new therapeutic target for HIV-1 and APOL1-associated nephropathies.

INTRODUCTION

HIV-associated nephropathy (HIVAN) is a kidney disease characterized by heavy proteinuria and rapid progression to chronic kidney failure if proper antiretroviral therapy (ART) is not available [1,2]. From the renal histological point of view, HIVAN is characterized by collapsing glomerulopathy, de-differentiation and proliferation of podocytes and glomerular parietal epithelial cells, development of focal and segmental glomerulosclerosis (FSGS), and microcystic dilatation of renal tubules leading to kidney enlargement [1,2]. People of African descents are at increased risk of developing HIVAN. In this regard, previous studies showed that two *Apolipoprotein L1* risk alleles (*APOL1-RA*), *G1* and *G2*, are strongly associated with the risk for people of African descent to develop HIVAN, as well as other chronic kidney diseases (CKD) [3,4]. Poorly controlled HIV infection is the most powerful factor known to contribute to APOL1- kidney diseases [4]. People living with HIV-1 carrying two copies of the *APOL1* RA have a ~50% lifetime risk of developing HIVAN [3]. However, to date, the basic mechanisms through which the APOL1-RA interacts with HIV to cause HIVAN are not clearly understood.

Mice do not have an ortholog to the human *APOL1* gene and cannot be infected with HIV. Nonetheless, APOL1 and HIV transgenic mouse models have been used to characterize the molecular mechanism through which the APOL1-RA and HIV-1 genes induce renal diseases. Functional studies to date exploring how APOL1 interacts with HIV have been limited to cell culture models and HIV-transgenic (Tg) mice and rats [5,6]. HIV-Tg26 mice and rats carrying a replication defective HIV construct driven by the HIV-LTR that lacks a 3kb sequence containing the *gag* and *pol* HIV genes (which are essential for viral replication), showed that the expression of HIV-genes in podocytes and tubular epithelial cells plays a critical role in inducing HIVAN in rodents [7–12]. In addition, follow up studies in several HIV-Tg mouse models showed that the HIV accessory protein negative factor (Nef), is a key determinant of the pathogenesis of HIVAN [7–12]. Nonetheless, in the absence of APOL1, other genetic factors are

needed to facilitate the development of HIVAN in mice [13]. Previous studies in cultured kidney cells as well as *APOL1* Tg mice and flies, have shown that the expression levels and localization of APOL1 are crucial in determining its cytotoxicity [14–17]. Yet, different dual APOL1-HIV-Tg26 mouse models have generated conflicting results, supporting toxicity or protection [14,18], and it remains unclear whether HIV-1 Nef interacts with the APOL1-RA directly to induce HIVAN. Thus, new animal models are needed to determine whether HIV-1 and APOL1 can interact in a simultaneous and cell type specific manner.

Drosophila is an established model for kidney diseases and development [15,19–24]. Its nephrocytes, equivalent to mammalian podocytes, contain a filtration structure made of lacuna channels and a basement membrane[25–28]. Moreover, nephrocytes and podocytes have many molecular similarities, including the importance of endocytosis and exocytosis for the formation and maintenance of their slit diaphragm filtration structures [25–28]. Furthermore, many of the genes associated with kidney diseases not only have functional homologs in *Drosophila*, but these homologous genes are required for nephrocyte function [20,24]. In this capacity, *Drosophila* nephrocytes have been used successfully to study the pathogenesis of *APOL1*-associated nephropathies [15,22,23,29,30]. Therefore, since APOL1-G1 is the most frequent risk variant present in African Americans living with HIVAN, we generated Tg flies expressing HIV-1 *nef* and *APOL1-G1* specifically in nephrocytes. Our findings suggest that Nef and APOL1-G1 act synergistically to induce nephrocyte cell death through the ER stress pathway, providing a potential therapeutic target for HIV-1 and APOL1-associated nephropathies.

145 **METHODS**

146

147 **Fly strains**

148 Flies were crossed, reared, and kept on standard food (Meidi LLC) at 22°C under standard
149 conditions. The following *Drosophila* lines were obtained from the Bloomington Drosophila
150 Stock Center (BDSC; Indiana University, IN): *Dot*-Gal4 (ID 6903; Ugt36A1 driver), UAS-YFP-
151 *Rab5* (ID 24616), UAS-YFP-*Rab7* (ID 23270), UAS-mCherry-*Atg8a* (ID 37750), and w^{1118}
152 (BDSC; ID 3605) which were used in the crosses. The *Hand*-GFP line (express green
153 fluorescent protein in the nuclei of nephrocytes and cardiomyocytes) was previously
154 generated by our team [31].

155

156 **DNA cloning and generation of transgenic fly strains**

157 The APOL1-G0 and APOL1-G1 *Drosophila* lines were generated as described before [15].
158 Briefly, the APOL1-G1 cDNA was obtained from a cDNA library generated from podocytes
159 cultured from a child with HIV-associated nephropathy, as described by Xie et al. [11], and differs
160 from the wild-type APOL1-G0 (AAI43040) only at S342 and I384. The HIV-1 Nef cDNA
161 (pGM91) was obtained from the NIH AIDS Research and Reference Reagent Program
162 (contributed by Dr. John Rossi) [32]. To generate UAS-*nef* constructs, the above cDNAs of the
163 *nef* allele were cloned into the pUASTattB vector and the transgene was introduced into a
164 fixed chromosomal docking site by germline transformation.

165

166 **10 kD dextran and FITC-albumin uptake assay**

167 20-day-old female flies from the *Dot*-Gal4 transgenic lines expressing UAS-*APOL1-G1* were
168 crossed with UAS-*nef* transgenic flies at 22°C. Dextran and albumin uptake by nephrocytes
169 was assessed ex vivo in adult flies by dissecting heart tissues in artificial hemolymph [70
170 mmol/l NaCl (Carolina), 5 mmol/l KCl (Sigma), 1.5 mmol/l $CaCl_2 \cdot 2H_2O$ (Sigma-Alrich), 4 mmol/l
171 $MgCl_2$ (Sigma-Aldrich), 10 mmol/l $NaHCO_3$ (Sigma-Aldrich), 5 mmol/l trehalose (Sigma), 115
172 mmol/l sucrose (Sigma-Aldrich), and 5 mmol/l HEPES (Sigma-Aldrich), in H_2O] and examining

173 cells by fluorescence microscopy after 20 minutes of incubation with Texas Red-dextran (10
174 kD, 0.05 mg/ml, Invitrogen) or FITC-albumin (100 mM, Sigma-Aldrich) and 10 minutes fixation
175 in 4% paraformaldehyde in phosphate buffered saline (1xPBS, Thermo Fisher Scientific). The
176 nephrocytes were mounted with Vectashield mounting medium (H-1000, Vector Laboratories).
177 For quantification, 40 nephrocytes were analyzed from 6 female flies per genotype.
178
179 **Nephrocyte size and number**
180 For this in vivo assay, we dissected 20-day-old adult female flies. The flies were from the *Dot*-
181 Gal4 transgenic lines that expressed UAS-APOL1-G0 or UAS-APOL1-G1 were crossed with
182 flies from the UAS-nef transgenic line at 22°C. The nephrocytes were dissected and kept in
183 artificial hemolymph [70 mmol/L NaCl (Carolina), 5 mmol/L KCl (Sigma), 1.5 mmol/L
184 $CaCl_2.2H_2O$ (Sigma-Aldrich), 4 mmol/L $MgCl_2$ (Sigma-Aldrich), 10 mmol/L $NaHCO_3$ (Sigma-
185 Aldrich), 5 mmol/L trehalose (Sigma), 115 mmol/L sucrose (Sigma-Aldrich), and 5 mmol/L
186 HEPES (Sigma-Aldrich), in H_2O], followed by a 10 minutes fixation in 4% paraformaldehyde
187 in 1XPBS (Thermo scientific). Images were obtained by confocal microscopy (ZEISS LSM
188 900; see details below). Nephrocyte size was determined using the area measurement
189 function in ImageJ [33] (version 1.52a), whereas nephrocyte numbers were manually counted in
190 the same fluorescent images. For quantitation of nephrocyte size, 40 nephrocytes were
191 analyzed from 6 female flies per genotype. For quantitation of nephrocyte number, 10 female
192 flies were analyzed per genotype.
193
194 **Fluorescent immunochemistry**
195 For Polychaetoid (Pyd) immunochemistry, 20-day-old female flies were dissected and heat-
196 fixed for 20 seconds in 100°C artificial hemolymph [70 mmol/l NaCl (Carolina), 5 mmol/l KCl
197 (Sigma), 1.5 mmol/l $CaCl_2{\cdot}2H_2O$ (Sigma-Alrich), 4 mmol/l $MgCl_2$ (Sigma-Aldrich), 10 mmol/l
198 $NaHCO_3$ (Sigma-Aldrich), 5 mmol/l trehalose (Sigma), 115 mmol/l sucrose (Sigma-Aldrich),
199 and 5 mmol/l HEPES (Sigma-Aldrich), in H_2O]. Primary mouse monoclonal anti-Pyd antibody
200 (PYD2) was obtained from Developmental Studies Hybridoma Bank and was used at 1:100

201 dilutions in 1xPBS with 0.1% Triton X-100 (Sigma) (PBST). The secondary antibody Alexa
202 Fluor 555 (A-21422, Thermo Fisher Scientific) was used diluted 1:1,000 in PBST. The
203 nephrocytes were washed with PBST three times, blocked in PBST+2% bovine serum albumin
204 (BSA; Sigma-Aldrich) for 40 min, incubated with primary antibody overnight at 4°C. Next day,
205 washed with PBST three times, incubated with secondary antibody for 2 hrs at room
206 temperature, washed with PBST three times, and mounted with Vectashield mounting medium
207 (H-1000, Vector Laboratories). 40 nephrocytes were analyzed from 6 female flies per
208 genotype.
209
210 For Ref(2)p, ubiquitin (FK2), and PDI immunochemistry, 20-day-old female flies were
211 dissected and fixated for 10 min in 4% paraformaldehyde in 1xPBS (Thermo Fisher Scientific).
212 Primary antibodies were diluted in PBST: Rabbit polyclonal antibody against Ref(2)P (1:100)
213 (ab178440, Abcam); Monoclonal mouse antibody ubiquitin FK2, raised against human
214 polyubiquitin-B and polyubiquitin-C (1:100) (BML-PW8810, Enzo Life Sciences); Rabbit
215 polyclonal antibody against protein disulfide isomerase (1:100) (PDI; P7122, Sigma).
216 Secondary antibody Alexa Fluor 555 (A-21422, Thermo Fisher Scientific) was used at 1:1,000
217 dilution in PBST. The nephrocytes were washed with PBST three times, blocked in PBST+2%
218 BSA (Sigma-Aldrich) for 40 min, incubated with primary antibodies overnight at 4°C. Next day,
219 washed with PBST three times, incubated with secondary antibody for 2 hrs at room
220 temperature, washed with 1xPBST three times, and mounted with Vectashield mounting
221 medium (H-1000, Vector Laboratories). For quantitation, 40 nephrocytes were analyzed from
222 6 female flies per genotype.
223
224 **Imaging of tagged protein**
225 For Rab5-GFP, Rab7-GFP, and Atg8a-mCherry imaging, 20-day-old adult flies (female) that
226 expressed the protein of interest with a fluorescent tag in their nephrocytes were dissected in
227 artificial hemolymph [70 mmol/L NaCl (Carolina), 5 mmol/L KCl (Sigma), 1.5 mmol/L
228 $CaCl_2.2H_2O$ (Sigma-Aldrich), 4 mmol/L $MgCl_2$ (Sigma-Aldrich), 10 mmol/L $NaHCO_3$ (Sigma-

229 Aldrich), 5 mmol/L trehalose (Sigma), 115 mmol/L sucrose (Sigma-Aldrich), and 5 mmol/L
230 HEPES (Sigma-Aldrich), in H_2O]. The nephrocytes were kept in artificial hemolymph and
231 imaged live.
232
233 **LysoTracker assay**
234 20-day-old female flies from the *Hand*-GFP and *Dot*-Gal4 transgenic lines expressing UAS-
235 *APOL1-G1* were crossed with UAS-*nef* transgenic flies at 22°C. LysoTracker intensity by
236 nephrocytes was assessed ex vivo in adult flies by dissecting heart tissues in artificial
237 hemolymph [70 mmol/l NaCl (Carolina), 5 mmol/l KCl (Sigma), 1.5 mmol/l $CaCl_2 \cdot 2H_2O$ (Sigma-
238 Alrich), 4 mmol/l $MgCl_2$ (Sigma-Aldrich), 10 mmol/l $NaHCO_3$ (Sigma-Aldrich), 5 mmol/l
239 trehalose (Sigma), 115 mmol/l sucrose (Sigma-Aldrich), and 5 mmol/l HEPES (Sigma-Aldrich),
240 in H_2O] and examining cells by fluorescence microscopy after 20 minutes incubation with
241 LysoTracker (Red DND-99, Thermo Fisher Scientific) used according to manufacturer
242 instructions and 10 minutes fixation in 4% paraformaldehyde in 1xPBS (Thermo Fisher
243 Scientific). For quantification, 40 nephrocytes were analyzed from 6 female flies per genotype.
244 The nephrocytes were mounted with VectaShield mounting medium (H-1000, Vector
245 Laboratories). For quantification, 40 nephrocytes were analyzed from 6 female flies per
246 genotype.
247
248 **TUNEL assay**
249 Terminal deoxynucleotidyl transferase dUTP nick end labeling (TUNEL) assay detects DNA
250 fragmentation by labeling the 3′-hydroxyl termini in the double-strand DNA breaks generated
251 during apoptosis. 20-day-old female flies were dissected in 100 °C artificial hemolymph [70
252 mmol/l NaCl (Carolina), 5 mmol/l KCl (Sigma), 1.5 mmol/l $CaCl_2 \cdot 2H_2O$ (Sigma-Alrich), 4 mmol/l
253 $MgCl_2$ (Sigma-Aldrich), 10 mmol/l $NaHCO_3$ (Sigma-Aldrich), 5 mmol/l trehalose (Sigma), 115
254 mmol/l sucrose (Sigma-Aldrich), and 5 mmol/l HEPES (Sigma-Aldrich), in H_2O] and heat-fixed
255 for 20 min in 4% paraformaldehyde in PBS (Thermo Fisher Scientific). The nephrocytes were
256 blocked with blocking buffer [50 mM Tris-Cl (pH 7.4) (Sigma-Alrich), 0.1% Triton X-100

257 (Sigma), and 188 mM NaCl (Carolina), in H_2O] and incubated with In Situ Cell Death detection
258 kit (Roche) used according to manufacturer instructions. The nephrocytes were mounted with
259 Vectashield mounting medium (H-1000, Vector Laboratories). 40 nephrocytes were analyzed
260 from 6 female flies per genotype.
261
262 **Confocal imaging**
263 Images for 10 kD dextran and FITC-albumin uptake and LysoTracker assays were obtained
264 using a ZEISS LSM900 microscope with a 20× Plan-Apochromat 0.8 NA air objective (ZEN
265 Blue, edition 3.0, acquisition software). Fluorescent immunochemistry confocal images for
266 anti-Pyd, anti-Ref(2)P, anti-PDI, anti-ubiquitin (anti-Fk2), and TUNEL were obtained using the
267 ZEISS LSM900 confocal microscope with a 63× Plan-Apochromat 1.4 NA oil objective under
268 AiryScan SR mode (ZEN Blue, edition 3.0, acquisition software). Live-cell fluorescence
269 confocal images for the UAS-YFP-*Rab5*, UAS-YFP-*Rab7*, and UAS-mCherry-*Atg8a* fly lines
270 were obtained with a ZEISS LSM900 confocal microscope with a 63× Plan-Apochromat 1.4
271 NA oil objective under AiryScan SR mode (ZEN Blue, edition 3.0, acquisition software). For
272 quantitative comparison of intensities, common settings were chosen to avoid oversaturation
273 and then applied across images for all samples within an assay. ImageJ [33] software (version
274 1.52a) was used for all image processing.
275
276 **Statistical analysis**
277 Statistical tests were performed using PAST.exe software [Natural History Museum, University
278 of Oslo (UiO), Oslo, Norway]. Data were first tested for normality using the Shapiro-Wilk test
279 (α=0.05). Normally distributed data were analyzed by one-way ANOVA followed by Tukey-
280 Kramer post-test for comparing multiple groups. Non-normal distributed data were analyzed
281 Kruskal-Wallis H-test followed by a Dunn's test for comparisons between multiple groups. The
282 results are presented as mean ± s.d. Statistical significance was determined as $P<0.05$.
283 Details for sample size used for quantitation are provided in the figure legends. The statistical
284 tests applied to determine significance are provided in Supplementary File 1.

285 **RESULTS**

286

287 **APOL1-G1-induced nephrocyte dysfunction was exacerbated by HIV-1 Nef**

288 In a previous study, we described the generation of transgenic *Drosophila* lines carrying the
289 human *APOL1-G0* wild-type allele or the *APOL1-G1* risk-allele (RA) derived from a child with
290 HIV-associated nephropathy [15]. Here, to define how HIV-1 Nef affects the structure and
291 function of nephrocytes, we generated additional transgenic fly lines that express HIV-1 *nef*
292 specifically in the nephrocytes and explored its role alone or in combination with *APOL1-G0*
293 or *APOL1-G1*.

294

295 To measure functional changes induced by nephrocyte-specific *APOL1* expression together
296 with HIV-1 *nef*, we used an ex vivo functional assay that measures the capacity of dissected
297 nephrocytes to filter and endocytose 10 kD fluorescent dextran or FITC-albumin particles. HIV-
298 1 *nef* or *APOL1-G0* by itself did not show a reduction in 10 kD dextran or FITC-albumin uptake
299 compared to control nephrocytes (Figure 1A, B, and C). Nephrocytes that expressed *nef* and
300 *APOL1* combined (*APOL1-G0+nef* or *APOL1-G1+nef*), showed a significant decreased
301 uptake of 10 kD dextran and FITC-albumin compared to those that express either *nef, APOL1-*
302 *G0*, or *APOL1-G1* alone (Figure 1A, B and C). The uptake of either 10 kD dextran or FITC-
303 albumin was significantly reduced in *APOL1-G1+nef* Tg flies, when compared to *APOL1-*
304 *G0+nef* flies (Figure 1A, B and C), thus reflecting the higher toxicity of the *APOL1-G1* risk
305 allele. In summary, these results show that HIV-1 Nef exacerbates APOL1-induced
306 nephrocyte dysfunction.

307

308 **Combined HIV-1 Nef and APOL1 exacerbated nephrocyte hypertrophy and cell death**

309 Previously, we showed that the expression of *APOL1-G1* in nephrocytes induced progressive
310 hypertrophy and accelerated their death [15]. Here, we confirmed that the expression of APOL-
311 G1 in aged flies (20-day-old) also increased the size of nephrocytes (Figure 1D). In contrast,
312 nephrocytes expressing HIV-1 *nef* or *APOL1-G0* alone, did not show a significant increase in

313 cell size (Figure 1D), while those that expressed *nef* combined with either *APOL1-G0* or
314 *APOL1-G1* were significantly larger (*APOL1-G0+nef* or *APOL1G1+nef*; Figure 1D).
315 Furthermore, nephrocytes expressing *nef* and *APOL1-G1* were larger than those expressing
316 *nef* and *APOL1-G0* combined (Figure 1D).
317
318 Like before [15], we observed reduced nephrocyte numbers in aged (20-day-old) Tg flies
319 expressing *APOL1-G1* (Figure 1E). However, we did not observe significant changes in the
320 number of nephrocytes in flies expressing HIV-1 *nef* or *APOL1-G0* alone (Figure 1E). In
321 contrast, flies expressing *nef* combined with *APOL1-G0* or *APOL1-G1*, showed a significant
322 reduction in the nephrocyte number when compared to those expressing *APOL1-G0* or
323 *APOL1-G1* alone (Figure 1E). Moreover, nephrocyte numbers were significantly reduced in
324 flies expressing *nef* and *APOL1-G1* combined, when compared to those expressing both *nef*
325 and *APOL1-G0 together* (Figure 1E). These results show that HIV-1 Nef combined with
326 APOL1-G1 further exacerbates the damage and loss of nephrocytes.
327
328 **HIV-1 Nef and APOL1-G1 combined disrupt the slit diaphragm filtration structure**
329 The slit diaphragm in *Drosophila* is a highly organized structure that plays a critical role
330 maintaining the filtration function of nephrocytes [25]. To determine whether the changes
331 induced by HIV-1 Nef in the uptake of 10 kD dextran were accompanied by an altered
332 nephrocyte filtration structure, we assessed the localization of the slit diaphragm protein
333 polychaetoid (Pyd - the homolog of human tight junction protein ZO-1) [27]. As expected, control
334 nephrocytes showed the typical fingerprint-like localization pattern of Pyd on their cell surface
335 (Figure 2A). In the optical medial view, control healthy nephrocytes also showed the
336 characteristic continuous circular ring expression pattern of Pyd (Figure 2B). Notably,
337 nephrocytes that expressed *nef* or *APOL1-G0* alone did not show a visible disruption of Pyd
338 (Figure 2A and B). However, nephrocytes that expressed *nef* combined with *APOL1-G0* or
339 *APOL1-G1* showed highly disorganized Pyd localization, more so than either APOL-1 risk
340 variant alone. Moreover, mislocalized Pyd was more evident in nephrocytes that expressed

341 both *nef* and *APOL1-G1* together, when compared to those expressing combined *nef* and
342 *APOL1-G0* (Figure 2A and B). In agreement with the altered uptake observed in nephrocytes
343 expressing *nef* and *APOL1* combined (Figure 1), these data demonstrate that both genes
344 acting together affect the localization of Pyd and disrupt the slit diaphragm filtration structure
345 of nephrocytes.
346
347 **Combined HIV-1 Nef and APOL1-G1 exacerbated the detrimental effects on nephrocyte**
348 **endocytosis**
349 Previously, we showed that HIV-1 can infect cultured human podocytes via dynamin-
350 dependent endocytosis in a process that is facilitated by transmembrane TNF-α [5]. To examine
351 whether HIV-1 Nef and APOL1 interact to regulate this process in fly nephrocytes, we assayed
352 the expression level of the early and late endosomal markers, Rab5 and Rab7, respectively.
353 Expression of *nef*, *APOL1-G0* or *APOL1-G1* alone, or combined did not induce significant
354 changes in the expression levels or localization of Rab5 (Figure 3A and B). In contrast, Rab7
355 protein expression levels were significantly increased in nephrocytes that expressed *APOL1-*
356 *G1*, but not in those expressing *nef* or *APOL1-G0* alone (Figure 3C and D). Nephrocytes that
357 expressed *nef* combined with *APOL1-G0* or *APOL1-G1* had significantly higher Rab7 protein
358 expression levels (Figure 3C and D). Moreover, the highest Rab7 protein expression levels
359 were observed in flies that expressed *nef* and *APOL1-G1* combined, when compared to all
360 other flies (Figure 3C and D).
361
362 We had also shown previously that *APOL1-G1* altered the acidification of organelles and the
363 lysosomes in fly nephrocytes, which could impair their function [15]. Thus, here we used the
364 fluorescent LysoTracker dye to examine acidic vacuoles and lysosomes in nephrocytes
365 (Figure 3E). LysoTracker fluorescence intensity was significantly reduced in nephrocytes that
366 expressed *APOL1-G1*, but not *nef* or *APOL1-G0* (Figures 3E and F). Nephrocytes that
367 expressed *nef* combined with *APOL1-G0* or *APOL1-G1* showed significantly lower
368 LysoTracker fluorescence intensity levels (Figure 3E and F). Moreover, lower LysoTracker

369 fluorescence intensity was observed in nephrocytes from dual *APOL1-G1+nef* Tg flies, when
370 compared to any other fly (Figure 3E and F). Together these findings indicate that HIV-1 Nef
371 exacerbates the changes induced by APOL1-G1 in key endocytic and acidification pathways
372 that appear to be essential for the normal function of nephrocytes.
373
374 **HIV-1 Nef enhances APOL1-G1-induced autophagic changes leading to the**
375 **accumulation of autophagosomes in fly nephrocytes**
376 APOL1 has been shown to modulate autophagy in various experimental model systems
377 [14,16,22,29,34–36]. Autophagy-related 8a (Atg8a), the equivalent of human LC3 (officially known as
378 MAP1LC3A), is a widely used marker for studying autophagy in *Drosophila* because it allows
379 the visualization of all autophagic structures, including autophagosomes. Nephrocytes that
380 expressed *nef* alone did not show higher expression levels of Atg8a-mCherry compared to
381 controls, although those expressing *nef* together with *APOL1-G0* or with *APOL1-G1* showed
382 significantly higher expression levels of Atg8a-mCherry, with more significant changes in
383 *APOL1-G1+nef* dual Tg flies (Figure 4A and B). We also examined the expression levels of
384 the refractory to sigma P [Ref(2)P] protein, which is a receptor for cargo destined to be
385 degraded by autophagy [37]. We did not observe significant changes in Ref(2)P expression
386 levels in nephrocytes that expressed *nef* alone compared to controls (Figure 4C and D). In
387 contrast, Ref(2)P was significantly increased in nephrocytes that expressed *APOL1-G0* or
388 *APOL1-G1*, and these changes were exacerbated in dual Tg flies that expressed both *nef* and
389 *APOL-G1* (Figure 4C and D). In addition, we observed an increase in the accumulation of
390 ubiquitinylated proteins in nephrocytes expressing *APOL1-G1*, but not *nef* or *APOL1-G0*
391 compared to controls (Figure 4E and F). Moreover, more ubiquitinylated proteins were
392 accumulated in the nephrocytes of *APOL1-G1+nef* dual Tg flies when compared to the
393 *APOL1-G0+nef* dual Tg flies (Figure 4E and F). Combined these data demonstrate that HIV-
394 1 Nef markedly increases APOL1-induced autophagy changes in nephrocytes.
395
396

397 **HIV-1 Nef and APOL1-G1 induce ER stress in fly nephrocytes**

398 APOL1-G1 has been shown to elicit the endoplasmic reticulum (ER) stress response [23,29],
399 while HIV-1 Nef bound the ER chaperone Calnexin (CNX) to induce ER stress [38–40]. Therefore,
400 we assessed the expression levels of protein disulfide-isomerase (PDI), a marker of ER stress
401 in nephrocytes. We found a significant increase in PDI in nephrocytes that expressed *nef* alone
402 compared to controls (Figure 5A and B). This increase was significantly more substantial when
403 *APOL1* was expressed simultaneously with *nef*; even when compared to the changes detected
404 in *APOL1-G0+nef* dual Tg flies (Figure 5A and B). Furthermore, nephrocytes that expressed
405 *APOL1-G1*, but not *nef* or *APOL1-G0*, alone showed positive results in the TUNEL assay, an
406 indicator of DNA fragmentation and considered a marker of cell death (Figure 5C). Likewise,
407 TUNEL-positive nephrocytes were observed in nephrocytes that expressed combined *APOL1-*
408 *G0+nef* or *APOL1-G1+nef* (Figure 5C). These findings indicate that HIV-1 Nef alone can
409 induce ER stress in *Drosophila* nephrocytes in an autophagy-independent pathway, and that
410 Nef can also exacerbate the APOL1-G1-induced autophagy-dependent pathway to further
411 stimulates ER stress, leading to nephrocyte dysfunction and cell death.

412

413

414 **DISCUSSION**

415

416 We have developed a new *Drosophila* model system to explore how HIV-1 Nef and APOL1-
417 G1 interact in fly nephrocytes to affect the structure and function of these cells *in vivo*. In brief,
418 we found that HIV-1 Nef acts in a synergistic manner with APOL1-G1 to impair the function of
419 key endocytic, acidification, and autophagic pathways, thereby affecting the normal structure
420 and function of fly nephrocytes. Previous studies showed that HIV-1 Nef can induce ER stress
421 by binding a chaperon protein called Calnexin (CNX) [38–40]. On the other hand, APOL1 disrupts
422 autophagy at the point of endosome-lysosome transition, leading to the accumulation of
423 proteins in the ER and thus promoting ER stress [23,29]. Here, we showed that in addition to
424 causing ER stress by itself through an autophagy-independent pathway (likely by binding to

425 Calnexin homologs in nephrocytes), Nef also exacerbates the pathogenic effect of APOL1-G1
426 on the autophagy pathway which also leads to ER stress. This synergistic interactions
427 between HIV-1 Nef and APOL1-G1 culminate in cellular toxicity and the premature death of
428 nephrocytes (Figure 6). We anticipate that this new *Drosophila* model will provide a clinically
429 relevant experimental tool to identify novel genetic interactions through which HIV-1 Nef and
430 APOL1-G1 may affect the function and survival of human podocytes precipitating HIV-1 and
431 APOL1-associated kidney diseases.
432
433 It is worth noting that APOL1-G1-induced cytotoxicity is not exclusively dependent on the
434 nucleotide substitutions or deletions that define the G1 risk variant. Other components of the
435 APOL1 molecule, including the BH3 domain [23,41], exon 4-encoded sequences [34], and different
436 haplotypes [42], also affect the toxicity of APOL1 in renal cells. Because introducing *APOL1-G1*
437 mutations to unnatural haplotype backgrounds, e.g., an *APOL1-G0* reference haplotype, could
438 affect the toxicity of APOL1, we generated our Tg flies that express a common natural *APOL1-*
439 *G1* derived from podocytes cultured from a child with HIVAN [11]. This APOL1-G1 contains the
440 haplotypes (E150; I228; K255) and only differs at S342 and I384 from a common natural
441 APOL1-G0 haplotype used to generate the control flies. Notably, this APOL1-G0 control
442 haplotype is more toxic in cultured human kidney epithelial cells (HEK 293) than the reference
443 APOL1-G0 haplotype used in other studies [11,16,22,43–49]. Indeed, we previously found that the
444 ectopic expression of *APOL1-G0* (reference allele) in fly nephrocytes, also induced
445 nephrocyte toxicity, albeit less severe compared to the *APOL1-G1* (risk allele) [15,29].
446 Subsequently, we showed that reducing the expression levels of *APOL1-G0* in fly nephrocytes
447 by lowering the temperature to 22°C, eliminated *APOL1-G0* toxicity [30], hence in the current
448 study all fly experiments were conducted at 22°C (instead of the conventional 25°C) so that
449 *APOL1-G1*, but not *APOL1-G0*, remains toxic in nephrocytes. In addition, we found that Nef
450 together with APOL1-G0 also affected the function of nephrocytes, although these changes
451 were less severe when compared to nephrocytes that expressed Nef combined with APOL1-
452 G1. Overall, these findings agree with clinical studies that showed that people of West African

453 genetic ancestry living with a high HIV-1 viral load can develop HIVAN even if they do not
454 carry an *APOL1-RA*; however, those that carry a risk allele are at much higher risk [4].
455
456 Interestingly, one study in *APOL-1* Tg mice, with expression driven by the podocyte-specific
457 promoter of *nephrin* (*Nphs1*), crossbred with HIV-Tg26 mice, unexpectedly found that the
458 *APOL1* wild-type allele (*G0*) ameliorated the podocyte loss characteristic of HIVAN, while
459 *APOL1-G2* did not induce significant renal changes [18]. This study suggested that APOL1-G0
460 could play a protective role in the pathogenesis of HIVAN. However, subsequent studies in
461 *APOL1* Tg mice developed with a coisogenic bacterial artificial chromosome (BAC) harboring
462 either wild-type (*G0*), *G1* or *G2* human *APOL1*, showed that the renal disease phenotype was
463 greater in *G2*/*G2* transgenic mice, compared to *G1*/*G1*, and that *APOL1-G0* did not rescue
464 *APOL1-G1* or *APOL1-G2* induced kidney toxicity after these mice were injected with
465 Interferon-gamma (INF-γ) [17]. Likewise, in a previous study, we found that *APOL1-G2* Tg flies
466 developed more significant nephrocyte injury compared to the *APOL1-G1* Tg flies [29]. These
467 studies also confirmed that the renal toxicity of APOL1-RA is mainly a function of the APOL1
468 expression level in renal cells [17], explaining why some Tg mice with *APOL1* driven by
469 podocyte-specific promoters develop more significant renal injury than others [6,14,17,50]. Our
470 current data from dual HIV-1 *nef* + *APOL1-G0* Tg flies, do not support the hypothesis that G0
471 offers protection against HIV-1 Nef, since Nef combined with APOL1-G0 induced significant
472 nephrocyte dysfunction. A recent study on bioRxiv used dual BAC/*APOL1*-HIV-Tg26 mice, in
473 which the *APOL1* transgene is a 47 kb human cDNA that contains the sequence from
474 chromosome 22 within a BAC [51]. It likewise showed that *APOL1-G1* aggravated the renal
475 injury in HIV-Tg26 mice, and that *APOL1-G0* did not prevent or minimize HIVAN in these mice
476 [51]. Taken together, our findings suggest that HIV-1 Nef per se is an independent risk factor
477 and potential second hit for developing APOL1 nephropathies.
478
479 We found that Nef together with APOL1-G1, but not alone, disrupted the autophagy pathway
480 and increased the accumulation of Atg8a-positive autophagosomes in fly nephrocytes. In line

481 with these findings, several studies have shown that HIV-1 can restrict autophagy to promote
482 viral replication by inhibiting the fusion between autophagosomes and lysosomes [35,52–54]. For
483 example, Nef overexpression in human astrocytes led to increased ATG8/LC3 [53]. Likewise,
484 Nef caused a significant acidification defect in human and macaque cardiomyocytes, altering
485 the subcellular localization of Rab7, and inducing cardiotoxicity through dysregulation of
486 autophagy [54]. Alternatively, in several human cell lines, HIV-1 Nef reduced the fusion of
487 autophagosomes to lysosomes by interacting with Beclin1 (BECN1)/Rab7 and dysregulating
488 the activity of the transcription factor EB (TFEB), which plays a key role in lysosomal
489 biogenesis [55,56]. Together, these findings show that HIV-1 Nef mediated inhibition of
490 autophagic flux is conserved across cell types and species. We did not observe visible
491 changes in the structure and function of nephrocytes that expressed HIV-1 Nef alone. It is
492 possible that increasing the expression of Nef would lead to a mild phenotype, as previous
493 studies in podocyte-specific HIV-1 *nef* Tg mice have shown mild podocyte injury or de-
494 differentiation changes [9,57]. Notably, one study showed much more severe podocyte injury
495 when HIV-1 *nef* and *vpr* were expressed simultaneously in mouse podocytes, indicating a
496 synergistic interaction between these HIV-1 genes [9]. These findings suggest that other HIV-1
497 genes and cytokines are needed to evoke the complete phenotype of HIVAN in human
498 podocytes. On the other hand, Tg mice with HIV-1 *nef* driven by the CD4 promoter developed
499 kidney disease [12,58,59]. In this case, the podocytes did not express HIV-1 genes and showed
500 only mild changes, while renal infiltrating mononuclear cells that expressed HIV-1 *nef* showed
501 significant renal interstitial injury [12,58,59]. Nef, however, can be released by CD+ HIV-1 infected
502 cells predominately as a component of exosomes [60] and can also be taken up by uninfected
503 cells [61]. Therefore, the renal recruitment of CD4+ cells may facilitate the transfer of Nef to renal
504 epithelial cells.
505
506 Defective endosomal trafficking has been reported in yeast and flies that expressed *APOL1-*
507 *G1* [22]. Here, we demonstrated that APOL1-G1 impairs late endosome to lysosome transition
508 (Rab5 and Rab7) and thus the autophagy pathway [Atg8 and Ref(2)P]. Furthermore, Nef

509 enhanced the autophagic changes induced by APOL1-G1. Likewise, immunofluorescence
510 studies in cultured human podocytes derived from low-risk (*G0*/*G0*) and high-risk (*G1*/*G2*)
511 allele subjects revealed increased Rab7 (late endosomes) and LC3II (autophagosomes)
512 positive intracellular organelles in high-risk compared to low-risk allele podocytes [14]. Studies
513 in inducible podocyte-specific *APOL1-RA* transgenic mice also showed that G1 interferes with
514 intracellular vesicular trafficking by impairing endocytic, autophagic, and acidification
515 pathways, as well as by disrupting the maturation of autophagosomes and autophagic flux,
516 which correlated with the development of FSGS [14]. Indeed, both *APOL-1* risk alleles have
517 been shown to affect autophagy in cultured human podocytes [62,63].
518
519 Taken together, these studies suggest that the new *APOL1* and HIV-1 *nef* Tg fly models can
520 generate clinically relevant information for humans. However, the *APOL1+nef* Tg fly models
521 have several limitations as well. Firstly, the models are based on the ectopic overexpression
522 of *APOL1* haplotypes, which can affect APOL1 intracellular localization and cytotoxicity [7, 8].
523 Overexpression also bypasses the infection process as well as the effects of circulating
524 cytokines released by HIV-1 infected cells (e.g., TNF-α, INF-γ), which can act as a second hit.
525 On the other hand, our model permits the exploration of HIV-1 Nef and APOL1 interactions
526 independently of these confounding variables. Secondly, we explored only the interactions
527 between the APOL1-G1 and HIV-1 Nef, while other HIV-1 proteins (e.g., Vpr or Tat) acting
528 either independently or in synergy with Nef or APOL1 can play relevant roles the
529 pathomechanism underlying HIVAN. Thirdly, HIVAN is a complex disease, involving other
530 renal glomerular and tubular cell types besides podocytes, as well as lesions that cannot be
531 studied in flies (e.g., collapsing glomerulopathy). Nevertheless, based on the notion that the
532 relevant pathways are conserved in human podocytes, flies provide a unique opportunity to
533 perform rapid and cost-effective genetic screenings to uncover new genetic interactions and
534 pathways that are modulated by HIV-1 and APOL1.
535
536

537 **DISCLOSURES**

538

539 The authors declare no competing interests.

540

541

542 **FUNDING**

543

544 This work was supported by National Institutes of Health grants R01-DK115968 (P.E.R. and
545 Z.H.), R01-DK103564 (P.E.R.), R01-DK120908 (Z.H.), and R01-DK098410 (Z.H.).

546

547

548 **ACKNOWLEDGMENTS**

549

550 We thank the Bloomington Drosophila Stock Center (BDSC) based at Indiana University
551 (Bloomington, IN) for the *Drosophila* stocks; and the Developmental Studies Hybridoma Bank
552 (DSHB) based at the University of Iowa (Iowa City, IA) for providing the antibodies.

553

554

555 **AUTHOR CONTRIBUTIONS**

556

557 J.Z. and Z.H. designed the study; J.Z., Y.F., Y.Y. and JL. carried out the experiments; J.Z.,
558 J.vdL., and Z.H. analyzed and interpreted the data; J.Z. prepared the figures; J.Z, J.vdL., P.R.,
559 and Z.H. drafted and revised the manuscript; the manuscript has been critically reviewed and
560 the final version approved by all authors.

561

562

563

564

565 **REFERENCES**

566

567 1. Ross MJ: Advances in the pathogenesis of HIV-associated kidney diseases. *Kidney Int.*
568 86: 266–274, 2014

569 2. Swanepoel CR, Atta MG, D'Agati VD, Estrella MM, Fogo AB, Naicker S, et al.: Kidney
570 disease in the setting of HIV infection: conclusions from a Kidney Disease: Improving
571 Global Outcomes (KDIGO) Controversies Conference. *Kidney Int.* 93: 545–559, 2018

572 3. Kopp JB, Nelson GW, Sampath K, Johnson RC, Genovese G, An P, et al.: APOL1 genetic
573 variants in focal segmental glomerulosclerosis and HIV-associated nephropathy. *J. Am.*
574 *Soc. Nephrol.* 22: 2129–2137, 2011

575 4. Kasembeli AN, Duarte R, Ramsay M, Mosiane P, Dickens C, Dix-Peek T, et al.: APOL1
576 risk variants are strongly associated with HIV-associated nephropathy in black South
577 Africans. *J. Am. Soc. Nephrol.* 26: 2882–2890, 2015

578 5. Li J, Das JR, Tang P, Han Z, Jaiswal JK, Ray PE: Transmembrane TNF-α Facilitates HIV-
579 1 Infection of Podocytes Cultured from Children with HIV-Associated Nephropathy. *J. Am.*
580 *Soc. Nephrol.* 28: 862–875, 2017

581 6. Yoshida T, Latt KZ, Rosenberg AZ, Shrivastav S, Heymann J, Halushka MK, et al.:
582 Transcriptomic Analysis of Human Podocytes In Vitro: Effects of Differentiation and
583 APOL1 Genotype. *Kidney Int Rep* 8: 164–178, 2023

584 7. Kajiyama W, Kopp JB, Marinos NJ, Klotman PE, Dickie P: Glomerulosclerosis and viral
585 gene expression in HIV-transgenic mice: role of nef. *Kidney Int.* 58: 1148–1159, 2000

586 8. Ray PE, Liu X-H, Robinson LR, Reid W, Xu L, Owens JW, et al.: A novel HIV-1 transgenic
587 rat model of childhood HIV-1-associated nephropathy. *Kidney Int.* 63: 2242–2253, 2003

588 9. Zuo Y, Matsusaka T, Zhong J, Ma J, Ma L-J, Hanna Z, et al.: HIV-1 genes vpr and nef
589 synergistically damage podocytes, leading to glomerulosclerosis. *J. Am. Soc. Nephrol.*
590 17: 2832–2843, 2006

591 10. Lu T-C, He JC, Wang Z-H, Feng X, Fukumi-Tominaga T, Chen N, et al.: HIV-1 Nef
592 disrupts the podocyte actin cytoskeleton by interacting with diaphanous interacting
593 protein. *J. Biol. Chem.* 283: 8173–8182, 2008

594 11. Xie X, Colberg-Poley AM, Das JR, Li J, Zhang A, Tang P, et al.: The basic domain of HIV-
595 tat transactivating protein is essential for its targeting to lipid rafts and regulating fibroblast
596 growth factor-2 signaling in podocytes isolated from children with HIV-1-associated
597 nephropathy. *J. Am. Soc. Nephrol.* 25: 1800–1813, 2014

598 12. Hu C, Priceputu E, Cool M, Chrobak P, Bouchard N, Forestier C, et al.: NEF-Induced HIV-
599 Associated Nephropathy Through HCK/LYN Tyrosine Kinases. *Am. J. Pathol.* 193: 702–
600 724, 2023

601 13. Gharavi AG, Ahmad T, Wong RD, Hooshyar R, Vaughn J, Oller S, et al.: Mapping a locus
602 for susceptibility to HIV-1-associated nephropathy to mouse chromosome 3. *Proc. Natl.*
603 *Acad. Sci. U. S. A.* 101: 2488–2493, 2004

604 14. Beckerman P, Bi-Karchin J, Park ASD, Qiu C, Dummer PD, Soomro I, et al.: Transgenic
605 expression of human APOL1 risk variants in podocytes induces kidney disease in mice.
606 *Nat. Med.* 23: 429–438, 2017

607 15. Fu Y, Zhu J-Y, Richman A, Zhang Y, Xie X, Das JR, et al.: APOL1-G1 in Nephrocytes
608 Induces Hypertrophy and Accelerates Cell Death. *J. Am. Soc. Nephrol.* 28: 1106–1116,
609 2017

610 16. O'Toole JF, Schilling W, Kunze D, Madhavan SM, Konieczkowski M, Gu Y, et al.: ApoL1
611 Overexpression Drives Variant-Independent Cytotoxicity. *J. Am. Soc. Nephrol.* 29: 869–
612 879, 2018

613 17. McCarthy GM, Blasio A, Donovan OG, Schaller LB, Bock-Hughes A, Magraner JM, et al.:
614 Recessive, gain-of-function toxicity in an APOL1 BAC transgenic mouse model mirrors
615 human APOL1 kidney disease. *Dis. Model. Mech.* [Internet] 14: 2021 Available from:
616 http://dx.doi.org/10.1242/dmm.048952

617 18. Bruggeman LA, Wu Z, Luo L, Madhavan S, Drawz PE, Thomas DB, et al.: APOL1-G0
618 protects podocytes in a mouse model of HIV-associated nephropathy. *PLoS One* 14:
619 e0224408, 2019

620 19. Zhang F, Zhao Y, Han Z: An in vivo functional analysis system for renal gene discovery
621 in Drosophila pericardial nephrocytes. *J. Am. Soc. Nephrol.* 24: 191–197, 2013

622 20. Fu Y, Zhu J-Y, Richman A, Zhao Z, Zhang F, Ray PE, et al.: A Drosophila model system
623 to assess the function of human monogenic podocyte mutations that cause nephrotic
624 syndrome. *Hum. Mol. Genet.* 26: 768–780, 2017

625 21. Hermle T, Braun DA, Helmstädter M, Huber TB, Hildebrandt F: Modeling Monogenic
626 Human Nephrotic Syndrome in the Drosophila Garland Cell Nephrocyte. *J. Am. Soc.*
627 *Nephrol.* 28: 1521–1533, 2017

628 22. Kruzel-Davila E, Shemer R, Ofir A, Bavli-Kertselli I, Darlyuk-Saadon I, Oren-Giladi P, et
629 al.: APOL1-Mediated Cell Injury Involves Disruption of Conserved Trafficking Processes.
630 *J. Am. Soc. Nephrol.* 28: 1117–1130, 2017

631 23. Gerstner L, Chen M, Kampf LL, Milosavljevic J, Lang K, Schneider R, et al.: Inhibition of
632 endoplasmic reticulum stress signaling rescues cytotoxicity of human apolipoprotein-L1

633 risk variants in Drosophila. *Kidney Int.* [Internet] 2022 Available from:
634 http://dx.doi.org/10.1016/j.kint.2021.12.031

635 24. Rani L, Gautam NK: Drosophila Renal Organ as a Model for Identification of Targets and
636 Screening of Potential Therapeutic Agents for Diabetic Nephropathy. *Curr. Drug Targets*
637 19: 1980–1990, 2018

638 25. Weavers H, Prieto-Sánchez S, Grawe F, Garcia-López A, Artero R, Wilsch-Bräuninger
639 M, et al.: The insect nephrocyte is a podocyte-like cell with a filtration slit diaphragm.
640 *Nature* 457: 322–326, 2009

641 26. Zhuang S, Shao H, Guo F, Trimble R, Pearce E, Abmayr SM: Sns and Kirre, the
642 Drosophila orthologs of Nephrin and Neph1, direct adhesion, fusion and formation of a
643 slit diaphragm-like structure in insect nephrocytes. *Development* 136: 2335–2344, 2009

644 27. Wang L, Wen P, van de Leemput J, Zhao Z, Han Z: Slit diaphragm maintenance requires
645 dynamic clathrin-mediated endocytosis facilitated by AP-2, Lap, Aux and Hsc70-4 in
646 nephrocytes. *Cell Biosci.* 11: 83, 2021

647 28. Lang K, Milosavljevic J, Heinkele H, Chen M, Gerstner L, Spitz D, et al.: Selective
648 endocytosis controls slit diaphragm maintenance and dynamics in Drosophila
649 nephrocytes. *Elife* [Internet] 11: 2022 Available from:
650 http://dx.doi.org/10.7554/eLife.79037

651 29. Zhu J-Y, Lee J-G, Fu Y, van de Leemput J, Ray PE, Han Z: APOL1-G2 accelerates
652 nephrocyte cell death by inhibiting the autophagy pathway. *Dis. Model. Mech.* [Internet]
653 2023 Available from: http://dx.doi.org/10.1242/dmm.050223

654 30. Lee J-G, Fu Y, Zhu J-Y, Wen P, van de Leemput J, Ray PE, et al.: A SNARE protective
655 pool antagonizes APOL1 renal toxicity in Drosophila nephrocytes. *Cell Biosci.* 13: 199,
656 2023

657 31. Han Z, Olson EN: Hand is a direct target of Tinman and GATA factors during Drosophila
658 cardiogenesis and hematopoiesis. *Development* 132: 3525–3536, 2005

659 32. Murakawa GJ, Zaia JA, Spallone PA, Stephens DA, Kaplan BE, Wallace RB, et al.: Direct
660 detection of HIV-1 RNA from AIDS and ARC patient samples. *DNA* 7: 287–295, 1988

661 33. Schneider CA, Rasband WS, Eliceiri KW: NIH Image to ImageJ: 25 years of image
662 analysis. *Nat. Methods* 9: 671–675, 2012

663 34. Khatua AK, Cheatham AM, Kruzel ED, Singhal PC, Skorecki K, Popik W: Exon 4-encoded
664 sequence is a major determinant of cytotoxicity of apolipoprotein L1. *Am. J. Physiol. Cell*
665 *Physiol.* 309: C22-37, 2015

666 35. Chang C, Young LN, Morris KL, von Bülow S, Schöneberg J, Yamamoto-Imoto H, et al.:
667 Bidirectional Control of Autophagy by BECN1 BARA Domain Dynamics. *Mol. Cell* 73:
668 339-353.e6, 2019

669 36. Chun J, Zhang J-Y, Wilkins MS, Subramanian B, Riella C, Magraner JM, et al.:
670 Recruitment of APOL1 kidney disease risk variants to lipid droplets attenuates cell toxicity.
671 *Proc. Natl. Acad. Sci. U. S. A.* 116: 3712–3721, 2019

672 37. Gatica D, Lahiri V, Klionsky DJ: Cargo recognition and degradation by selective
673 autophagy. *Nat. Cell Biol.* 20: 233–242, 2018

674 38. Jennelle L, Hunegnaw R, Dubrovsky L, Pushkarsky T, Fitzgerald ML, Sviridov D, et al.:
675 HIV-1 protein Nef inhibits activity of ATP-binding cassette transporter A1 by targeting
676 endoplasmic reticulum chaperone calnexin. *J. Biol. Chem.* 289: 28870–28884, 2014

677 39. Ryan D, Carberry S, Murphy ÁC, Lindner AU, Fay J, Hector S, et al.: Calnexin, an ER-
678 induced protein, is a prognostic marker and potential therapeutic target in colorectal
679 cancer. *J. Transl. Med.* [Internet] 14: 2016 Available from:
680 http://dx.doi.org/10.1186/s12967-016-0948-z

681 40. Guérin R, Arseneault G, Dumont S, Rokeach LA: Calnexin is involved in apoptosis
682 induced by endoplasmic reticulum stress in the fission yeast. *Mol. Biol. Cell* 19: 4404–
683 4420, 2008

684 41. Heneghan JF, Vandorpe DH, Shmukler BE, Giovinazzo JA, Raper J, Friedman DJ, et al.:
685 BH3 domain-independent apolipoprotein L1 toxicity rescued by BCL2 prosurvival
686 proteins. *Am. J. Physiol. Cell Physiol.* 309: C332-47, 2015

687 42. Lannon H, Shah SS, Dias L, Blackler D, Alper SL, Pollak MR, et al.: Apolipoprotein L1
688 (APOL1) risk variant toxicity depends on the haplotype background. *Kidney Int.* 96: 1303–
689 1307, 2019

690 43. Lan X, Jhaveri A, Cheng K, Wen H, Saleem MA, Mathieson PW, et al.: APOL1 risk
691 variants enhance podocyte necrosis through compromising lysosomal membrane
692 permeability. *Am. J. Physiol. Renal Physiol.* 307: F326-36, 2014

693 44. Nichols B, Jog P, Lee JH, Blackler D, Wilmot M, D'Agati V, et al.: Innate immunity
694 pathways regulate the nephropathy gene Apolipoprotein L1. *Kidney Int.* 87: 332–342,
695 2015

696 45. Olabisi OA, Zhang J-Y, VerPlank L, Zahler N, DiBartolo S 3rd, Heneghan JF, et al.:
697 APOL1 kidney disease risk variants cause cytotoxicity by depleting cellular potassium
698 and inducing stress-activated protein kinases. *Proc. Natl. Acad. Sci. U. S. A.* 113: 830–
699 837, 2016

700 46. Granado D, Müller D, Krausel V, Kruzel-Davila E, Schuberth C, Eschborn M, et al.:
701 Intracellular APOL1 Risk Variants Cause Cytotoxicity Accompanied by Energy Depletion.
702 *J. Am. Soc. Nephrol.* 28: 3227–3238, 2017

703 47. Hayek SS, Koh KH, Grams ME, Wei C, Ko Y-A, Li J, et al.: A tripartite complex of suPAR,
704 APOL1 risk variants and αvβ3 integrin on podocytes mediates chronic kidney disease.
705 *Nat. Med.* 23: 945–953, 2017

706 48. Ma L, Chou JW, Snipes JA, Bharadwaj MS, Craddock AL, Cheng D, et al.: APOL1 Renal-
707 Risk Variants Induce Mitochondrial Dysfunction. *J. Am. Soc. Nephrol.* 28: 1093–1105,
708 2017

709 49. Wen H, Kumar V, Lan X, Shoshtari SSM, Eng JM, Zhou X, et al.: APOL1 risk variants
710 cause podocytes injury through enhancing endoplasmic reticulum stress. *Biosci. Rep.*
711 [Internet] 38: 2018 Available from: http://dx.doi.org/10.1042/BSR20171713

712 50. Bruggeman LA, Wu Z, Luo L, Madhavan SM, Konieczkowski M, Drawz PE, et al.: APOL1-
713 G0 or APOL1-G2 Transgenic Models Develop Preeclampsia but Not Kidney Disease. *J.*
714 *Am. Soc. Nephrol.* 27: 3600–3610, 2016

715 51. Yoshida T, Latt KZ, Santo BA, Shrivastav S, Zhao Y, Fenaroli P, et al.: APOL1 kidney risk
716 variants in glomerular diseases modeled in transgenic mice. *bioRxiv* [Internet] 2023
717 Available from: http://dx.doi.org/10.1101/2023.03.27.534273

718 52. Campbell GR, Rawat P, Bruckman RS, Spector SA: Human Immunodeficiency Virus
719 Type 1 Nef Inhibits Autophagy through Transcription Factor EB Sequestration. *PLoS*
720 *Pathog.* 11: e1005018, 2015

721 53. Saribas AS, Khalili K, Sariyer IK: Dysregulation of autophagy by HIV-1 Nef in human
722 astrocytes. *Cell Cycle* 14: 2899–2904, 2015

723 54. Gupta MK, Kaminski R, Mullen B, Gordon J, Burdo TH, Cheung JY, et al.: HIV-1 Nef-
724 induced cardiotoxicity through dysregulation of autophagy. *Sci. Rep.* 7: 8572, 2017

725 55. Franco-Juárez B, Coronel-Cruz C, Hernández-Ochoa B, Gómez-Manzo S, Cárdenas-
726 Rodríguez N, Arreguin-Espinosa R, et al.: TFEB; Beyond Its Role as an Autophagy and
727 Lysosomes Regulator. *Cells* [Internet] 11: 2022 Available from:
728 http://dx.doi.org/10.3390/cells11193153

729 56. Zhang W, Li X, Wang S, Chen Y, Liu H: Regulation of TFEB activity and its potential as a
730 therapeutic target against kidney diseases. *Cell Death Discov* 6: 32, 2020

731 57. Husain M, D'Agati VD, He JC, Klotman ME, Klotman PE: HIV-1 Nef induces
732 dedifferentiation of podocytes in vivo: a characteristic feature of HIVAN. *AIDS* 19: 1975–
733 1980, 2005

58. Hanna Z, Kay DG, Rebai N, Guimond A, Jothy S, Jolicoeur P: Nef harbors a major determinant of pathogenicity for an AIDS-like disease induced by HIV-1 in transgenic mice. *Cell* 95: 163–175, 1998

59. Hanna Z, Kay DG, Cool M, Jothy S, Rebai N, Jolicoeur P: Transgenic mice expressing human immunodeficiency virus type 1 in immune cells develop a severe AIDS-like disease. *J. Virol.* 72: 121–132, 1998

60. Dubrovsky L, Brichacek B, Prashant NM, Pushkarsky T, Mukhamedova N, Fleetwood AJ, et al.: Extracellular vesicles carrying HIV-1 Nef induce long-term hyperreactivity of myeloid cells. *Cell Rep.* 41: 111674, 2022

61. Mukhamedova N, Hoang A, Dragoljevic D, Dubrovsky L, Pushkarsky T, Low H, et al.: Exosomes containing HIV protein Nef reorganize lipid rafts potentiating inflammatory response in bystander cells. *PLoS Pathog.* 15: e1007907, 2019

62. Kumar V, Ayasolla K, Jha A, Mishra A, Vashistha H, Lan X, et al.: Disrupted apolipoprotein L1-miR193a axis dedifferentiates podocytes through autophagy blockade in an APOL1 risk milieu. *Am. J. Physiol. Cell Physiol.* 317: C209–C225, 2019

63. Ekulu PM, Adebayo OC, Decuypere J-P, Bellucci L, Elmonem MA, Nkoy AB, et al.: Novel human podocyte cell model carrying G2/G2 APOL1 high-risk genotype. *Cells* 10: 1914, 2021

765 **FIGURES**

766

767 **Figure 1. Expression of HIV-1 protein Nef facilitated nephrocyte function reduction,**
768 **hypertrophy, and cell death due to APOL1-G1.**

769 **(A-E)** Flies used (20-day-old adult females): Control (*Dot>w*^{1118}); *nef* (*Dot>nef*-OE); *APOL1-*
770 *G0* (*Dot>APOL1-G0*-OE); *APOL1-G1* (*Dot>APOL1-G1*-OE); *APOL1-G0+nef* (*Dot>APOL1-*
771 *G0*-OE+*nef*-OE); *APOL1-G1+nef* (*Dot>APOL1-G1*-OE+*nef*-OE). **(A) Top:** 10kD fluorescent
772 dextran particle uptake (red) by nephrocytes using nephrocyte specific driver *Dot*-Gal4 to
773 express HIV-1 *nef* alone or together with *APOL1-G0* and *APOL1-G1* at 22°C. Scale bar: 15
774 µm. **Bottom:** FITC-albumin particle uptake (green) by nephrocytes using nephrocyte
775 specifically driver *Dot*-Gal4 to express HIV-1 *nef* alone or together with *APOL1-G0* and
776 *APOL1-G1* at 22°C. Scale bar: 15 µm. **(B)** Quantitation of 10kD dextran uptake, relative to
777 uptake in control flies. n=40 nephrocytes from 6 flies, per group. **(C)** Quantitation of FITC-
778 albumin uptake, relative to uptake in control flies. n=40 nephrocytes from 6 flies, per group.
779 **(D)** Quantitation of adult nephrocyte size, relative to size in control flies. n=40 nephrocytes
780 from 6 flies, per group. **(E)** Quantitation of adult nephrocyte number, relative to cell number in
781 control flies. n=10 flies, per group. Results have been presented as mean ± s.d., normalized
782 to the control group. Kruskal–Wallis H-test followed by a Dunn's test; statistical significance:
783 *P<0.05, **P<0.01, ***P<0.001.

784

785

786

787

788

789

790

791

792

Figure 1

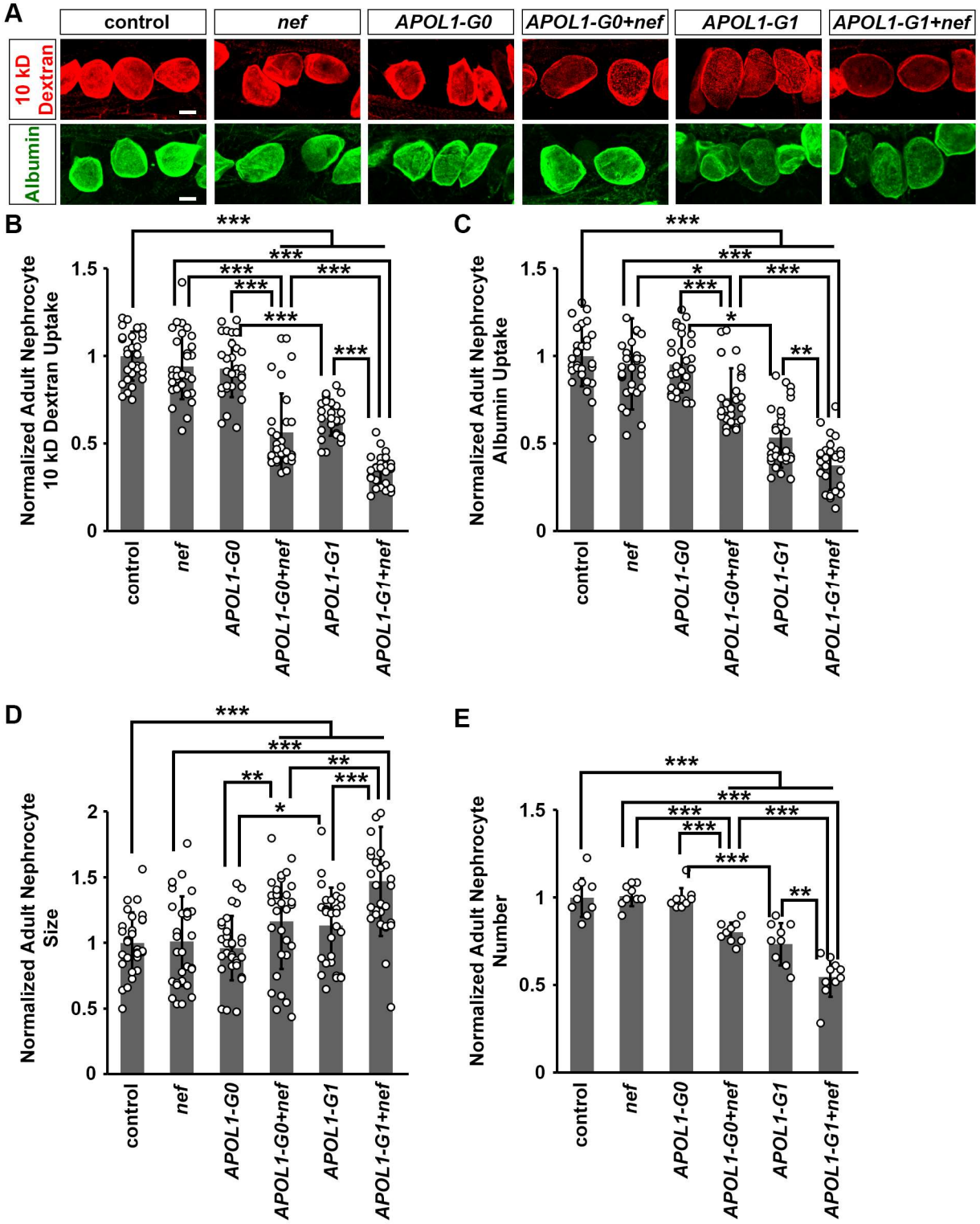
A
control
nef
APOL1-G0
APOL1-G0+nef
APOL1-G1
APOL1-G1+nef
10 kD Dextran
Albumin
B
Normalized Adult Nephrocyte 10 kD Dextran Uptake
C
Normalized Adult Nephrocyte Albumin Uptake
D
Normalized Adult Nephrocyte Size
E
Normalized Adult Nephrocyte Number

820 **Figure 2. The expression of HIV-1 protein Nef in nephrocytes facilitated the disruption**
821 **of the slit diaphragm due to APOL1-G1.**
822 **(A, B)** Flies used (20-day-old adult females): Control (*Dot>w*^{1118}); *nef* (*Dot>nef*-OE); *APOL1-*
823 *G0* (*Dot>APOL1-G0*-OE); *APOL1-G1* (*Dot>APOL1-G1*-OE); *APOL1-G0+nef* (*Dot>APOL1-*
824 *G0*-OE+*nef*-OE); *APOL1-G1+nef* (*Dot>APOL1-G1*-OE+*nef*-OE). **(A, B)** Localization of slit
825 diaphragm protein Polychaetoid (Pyd; red) at the surface (A) and medial (B) optical sections
826 in nephrocytes using the nephrocyte specific driver *Dot*-Gal4 to express HIV-1 *nef* alone or
827 together with *APOL1-G0* and *APOL1-G1* at 22°C. Boxed areas are shown magnified next to
828 each image. Scale bar: 5 μm; Scale bar (magnified): 1 μm.
829
830
831
832
833
834
835
836
837
838
839
840
841
842
843
844
845
846
847

Figure 2

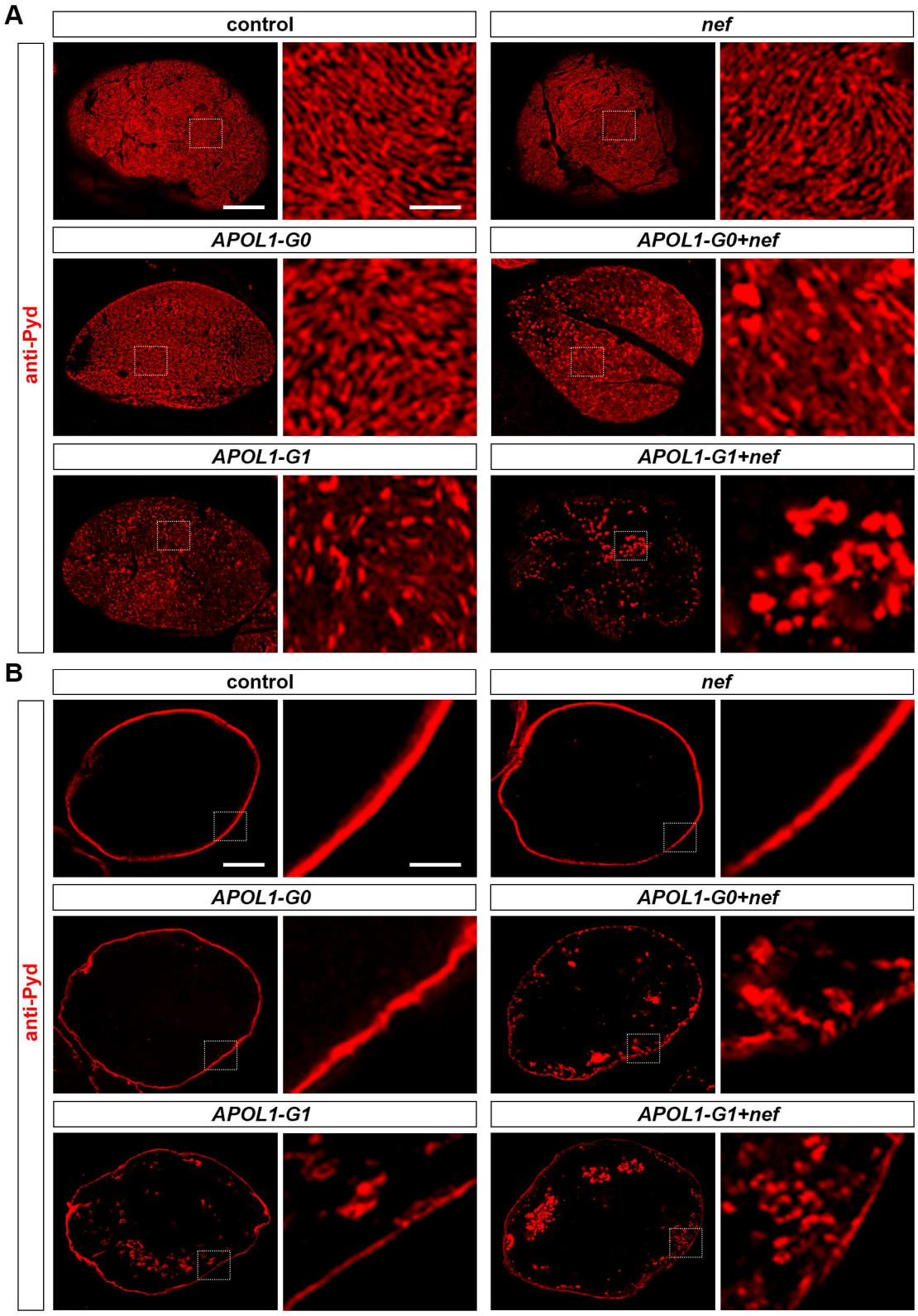
A
control
nef
anti-Pyd
APOL1-G0
APOL1-G0+nef
APOL1-G1
APOL1-G1+nef
B
control
nef
anti-Pyd
APOL1-G0
APOL1-G0+nef
APOL1-G1
APOL1-G1+nef

875 **Figure 3. The expression of HIV-1 protein Nef in nephrocytes facilitated the disruption**
876 **in endocytic membrane trafficking due to APOL1-G1.**
877 **(A, B)** Flies used (20-day-old adult females): Control (*Dot>Rab5*-YFP); *nef* (*Dot>Rab5*-YFP
878 +*nef*-OE); *APOL1-G0* (*Dot>Rab5*-YFP+*APOL1-G0*-OE); *APOL1-G1* (*Dot>Rab5*-
879 YFP+*APOL1-G1*-OE); *APOL1-G0+nef* (*Dot>Rab5*-YFP+*APOL1-G0*-OE+*nef*-OE); *APOL1-*
880 *G1+nef* (*Dot>Rab5*-YFP+*APOL1-G1*-OE+*nef*-OE). **(C, D)** Flies used (20-day-old adult
881 females): Control (*Dot>Rab7*-YFP); *nef* (*Dot>Rab7*-YFP +*nef*-OE); *APOL1-G0* (*Dot>Rab7*-
882 YFP+*APOL1-G0*-OE); *APOL1-G1* (*Dot>Rab7*-YFP+*APOL1-G1*-OE); *APOL1-G0+nef*
883 (*Dot>Rab7*-YFP+*APOL1-G0*-OE+*nef*-OE); *APOL1-G1+nef* (*Dot>Rab7*-YFP+*APOL1-G1*-
884 OE+*nef*-OE). **(E, F)** Flies used (20-day-old adult females): Control (*Hand*-GFP,
885 *Dot*>GFP+w^{1118}); *nef* (*Hand*-GFP*, Dot>nef*-OE); *APOL1-G0* (*Hand*-GFP*, Dot>APOL1-G0*-OE);
886 *APOL1-G1* (*Hand*-GFP*, Dot>APOL1-G1*-OE); *APOL1-G0+nef* (*Hand*-GFP, *Dot>APOL1-G0*-
887 OE+*nef*-OE); *APOL1-G1+nef* (*Hand*-GFP*, Dot>APOL1-G1*-OE+*nef*-OE). **(A)** Expression of
888 endocytosis-related proteins Rab5 (green, early endosome) in nephrocytes using the
889 nephrocyte specific driver *Dot*-Gal4 to express HIV-1 *nef* alone or together with *APOL1-G0*
890 and *APOL1-G1* at 22°C. Boxed areas are shown magnified next to each image. Scale bar: 5
891 μm; Scale bar (magnified): 1 μm. **(B)** Quantitation of Rab5 fluorescence intensity, relative to
892 fluorescence in control nephrocytes. n=40 nephrocytes from 6 flies, per group. Note: None of
893 the comparisons between groups were significant. **(C)** Expression of endocytosis-related
894 proteins Rab7 (green, late endosome) in nephrocytes using the nephrocyte specific driver *Dot*-
895 Gal4 to express HIV-1 *nef* alone or together with *APOL1-G0* and *APOL1-G1* at 22°C. Boxed
896 areas are shown magnified next to each image. Scale bar: 5 μm; Scale bar (magnified): 1 μm.
897 **(D)** Quantitation of Rab7 fluorescence intensity, relative to fluorescence in control
898 nephrocytes. n=40 nephrocytes from 6 flies, per group. **(E)** LysoTracker dye fluorescence level
899 (red) in nephrocytes using the nephrocyte specific driver *Dot*-Gal4 to express HIV-1 *nef* alone
900 or together with *APOL1-G0* and *APOL1-G1* at 22°C. *Hand*-GFP transgene expression was
901 visualized as green fluorescence concentrated in the nuclei of nephrocytes. Scale bar: 15 μm.
902 **(F)** Quantitation of LysoTracker dye fluorescence intensity, relative to fluorescence in control

903 nephrocytes. n=40 nephrocytes from 6 flies, per group. Results have been presented as mean
904 ± s.d., normalized to the control group. Kruskal–Wallis H-test followed by a Dunn's test;
905 statistical significance: *P<0.05, ***P<0.001.
906
907
908
909
910
911
912
913
914
915
916
917
918
919
920
921
922
923
924
925
926
927
928
929
930

Figure 3

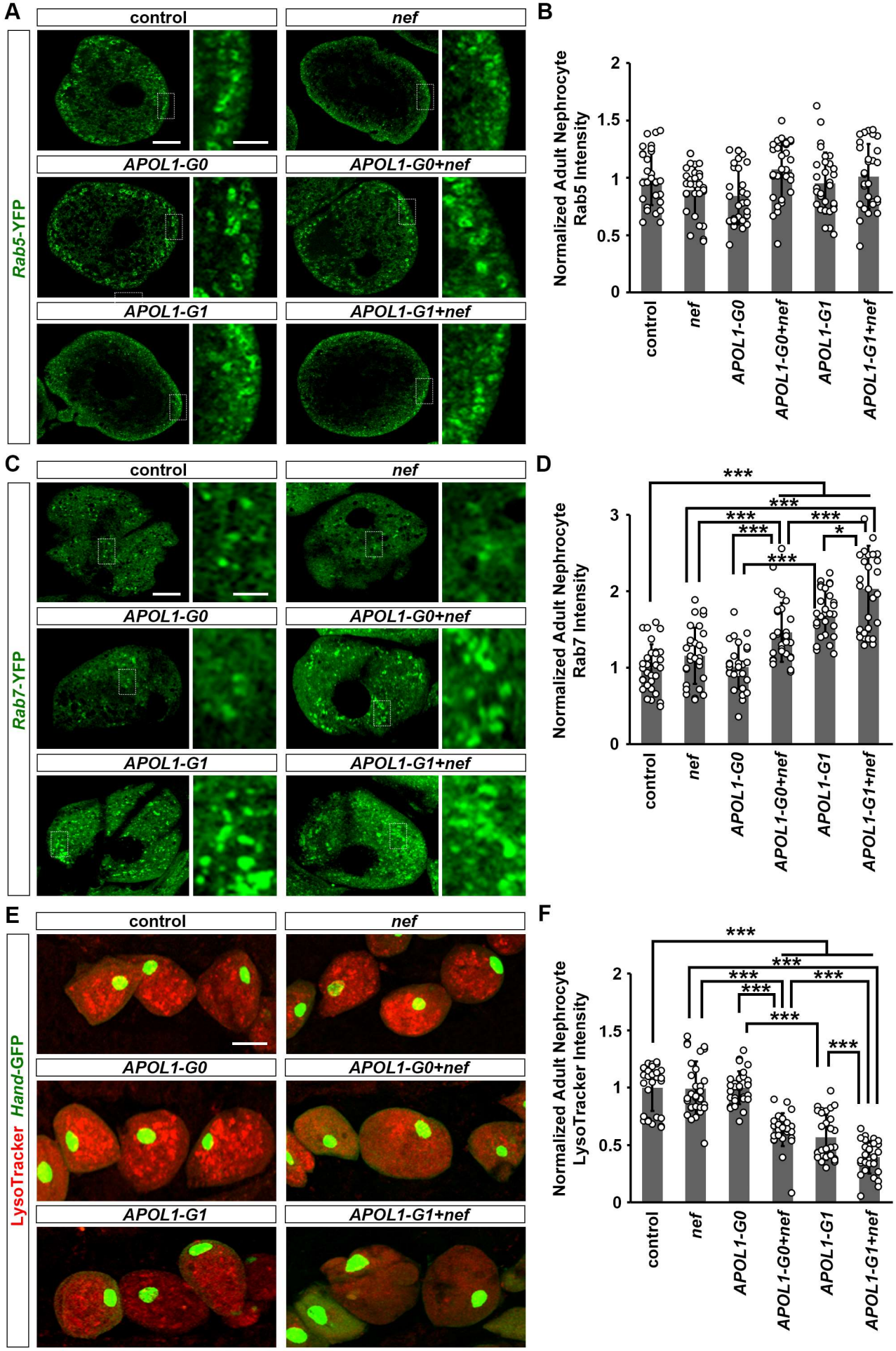
A
control
nef
APOL1-G0
APOL1-G0+nef
APOL1-G1
APOL1-G1+nef
Rab5-YFP
B
Normalized Adult Nephrocyte Rab5 Intensity
2
1.5
1
0.5
0
control
nef
APOL1-G0
APOL1-G0+nef
APOL1-G1
APOL1-G1+nef
C
control
nef
APOL1-G0
APOL1-G0+nef
APOL1-G1
APOL1-G1+nef
Rab7-YFP
D
Normalized Adult Nephrocyte Rab7 Intensity
3
2
1
0
***
*
control
nef
APOL1-G0
APOL1-G0+nef
APOL1-G1
APOL1-G1+nef
E
control
nef
APOL1-G0
APOL1-G0+nef
APOL1-G1
APOL1-G1+nef
LysoTracker Hand-GFP
F
Normalized Adult Nephrocyte LysoTracker Intensity
2
1.5
1
0.5
0
***
control
nef
APOL1-G0
APOL1-G0+nef
APOL1-G1
APOL1-G1+nef

959 **Figure 4. The expression of HIV-1 protein Nef in nephrocytes facilitated autophagy**
960 **impairment due to APOL1-G1.**
961 **(A, B)** Flies used (20-day-old adult females): Control (*Dot>Atg8a*-mCherry); *nef* (*Dot>Atg8a*-
962 mCherry+*nef*-OE); *APOL1-G0* (*Dot>Atg8a*-mCherry+*APOL1-G0*-OE); *APOL1-G1* (*Dot>*
963 *Atg8a*-mCherry+*APOL1-G1*-OE); *APOL1-G0+nef* (*Dot>Atg8a*-mCherry+*APOL1-G0*-OE+*nef*-
964 OE); *APOL1-G1+nef* (*Dot>Atg8a*-mCherry +*APOL1-G1*-OE+*nef*-OE). **(C-F)** Flies used (20-
965 day-old adult females): Control (*Dot>w*^{1118}); *nef* (*Dot>nef*-OE); *APOL1-G0* (*Dot>APOL1-G0*-
966 OE); *APOL1-G1* (*Dot>APOL1-G1*-OE); *APOL1-G0+nef* (*Dot>APOL1-G0*-OE+*nef*-OE);
967 *APOL1-G1+nef* (*Dot>APOL1-G1*-OE+*nef*-OE). **(A)** Expression of autophagy-related protein
968 8a (Atg8a; red, mCherry) in nephrocytes using the nephrocyte specific driver *Dot*-Gal4 to
969 express HIV-1 *nef* alone or together with *APOL1-G0* and *APOL1-G1* at 22°C. Boxed areas
970 are shown magnified next to each image. Scale bar: 5 μm; Scale bar (magnified): 1 μm. **(B)**
971 Quantitation of Atg8a fluorescence intensity, relative to fluorescence in control nephrocytes.
972 n=40 nephrocytes from 6 flies, per group. **(C)** Autophagy receptor refractory to sigma P
973 (Ref(2)P; red) in nephrocytes using the nephrocyte specific driver *Dot*-Gal4 to express HIV-1
974 *nef* alone or together with *APOL1-G0* and *APOL1-G1* at 22°C. Boxed areas are shown
975 magnified next to each image. Scale bar: 5 μm; Scale bar (magnified): 1 μm. **(D)** Quantitation
976 of Ref(2)P fluorescence intensity, relative to fluorescence in control nephrocytes. n=40
977 nephrocytes from 6 flies, per group. **(E)** Expression of ubiquitinylated proteins (green) in
978 nephrocytes using the nephrocyte specific driver *Dot*-Gal4 to express HIV-1 *nef* alone or
979 together with *APOL1-G0* and *APOL1-G1* at 22°C. Boxed areas are shown magnified next to
980 each image. Scale bar: 5 μm; Scale bar (magnified): 1 μm. **(D)** Quantitation of ubiquitinylated
981 proteins fluorescence intensity, relative to fluorescence in control nephrocytes. n=40
982 nephrocytes from 6 flies, per group. Results have been presented as mean ± s.d., normalized
983 to the control group. Kruskal–Wallis H-test followed by a Dunn's test; statistical significance:
984 *P<0.05, **P<0.01, ***P<0.001.
985
986

Figure 4

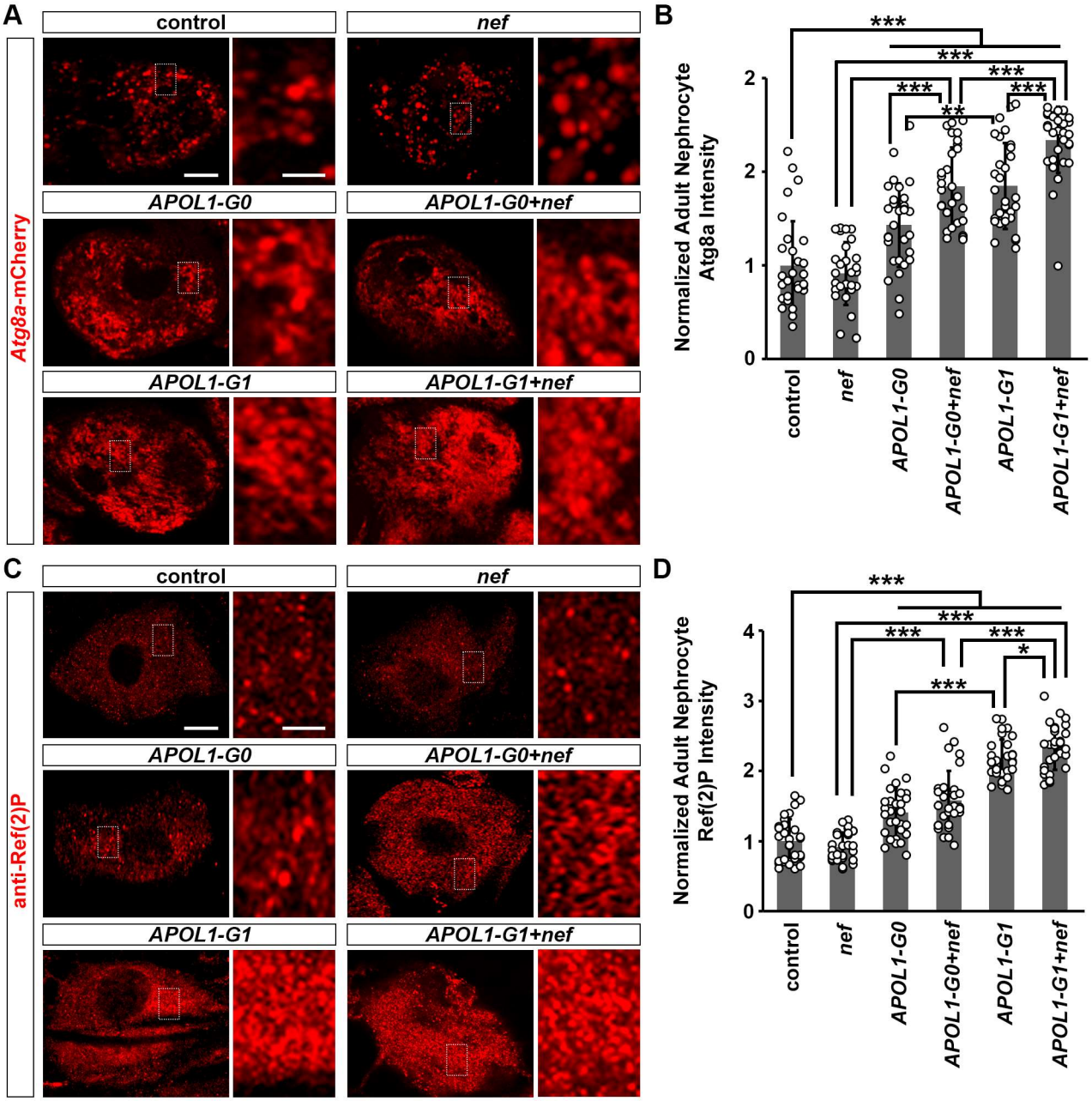
A
control
nef
APOL1-G0
APOL1-G0+nef
APOL1-G1
APOL1-G1+nef
Atg8a-mCherry
B
Normalized Adult Nephrocyte Atg8a Intensity
0
1
2
2
***
**
control
nef
APOL1-G0
APOL1-G0+nef
APOL1-G1
APOL1-G1+nef
C
control
nef
APOL1-G0
APOL1-G0+nef
APOL1-G1
APOL1-G1+nef
anti-Ref(2)P
D
Normalized Adult Nephrocyte Ref(2)P Intensity
0
1
2
3
4
***
*
control
nef
APOL1-G0
APOL1-G0+nef
APOL1-G1
APOL1-G1+nef

1015 **Figure 5. Expression of HIV-1 protein Nef in nephrocyte-induced ER stress.**

1016 **(A, B)** Flies used (20-day-old adult females): Control (*Dot*>w^{1118}); *nef* (*Dot*>*nef*-OE); *APOL1-*
1017 *G0* (*Dot*>*APOL1-G0*-OE); *APOL1-G1* (*Dot*>*APOL1-G1*-OE); *APOL1-G0+nef* (*Dot*>*APOL1-*
1018 *G0*-OE+*nef*-OE); *APOL1-G1+nef* (*Dot*>*APOL1-G1*-OE+*nef*-OE). **(C, D)** Flies used (20-day-
1019 old adult females): Control (*Hand*-GFP, *Dot*>GFP+w^{1118}); *nef* (*Hand*-GFP*, Dot*>*nef*-OE);
1020 *APOL1-G0* (*Hand*-GFP*, Dot*>*APOL1-G0*-OE); *APOL1-G1* (*Hand*-GFP*, Dot*>*APOL1-G1*-OE);
1021 *APOL1-G0+nef* (*Hand*-GFP, *Dot*>*APOL1-G0*-OE+*nef*-OE); *APOL1-G1+nef* (*Hand*-GFP*,*
1022 *Dot*>*APOL1-G1*-OE+*nef*-OE). **(A)** ER stress marker protein disulfide isomerase (PDI; red) in
1023 nephrocytes using the nephrocyte specific driver *Dot*-Gal4 to express HIV-1 *nef* alone or
1024 together with *APOL1-G0* and *APOL1-G1* at 22°C. Scale bar: 15 μm. **(B)** Quantitation of PDI
1025 fluorescence intensity, relative to fluorescence in control nephrocytes. n=40 nephrocytes from
1026 6 flies, per group. **(C)** Cell apoptosis marker TUNEL (red) in nephrocytes using the nephrocyte
1027 specific driver *Dot*-Gal4 to express HIV-1 *nef* alone or together with *APOL1-G0* and *APOL1-*
1028 *G1* at 22°C. *Hand*-GFP transgene expression was visualized as green fluorescence
1029 concentrated in the nuclei of nephrocytes. Scale bar: 5 μm.

1030
1031
1032
1033
1034
1035
1036
1037
1038
1039
1040
1041
1042

Figure 5

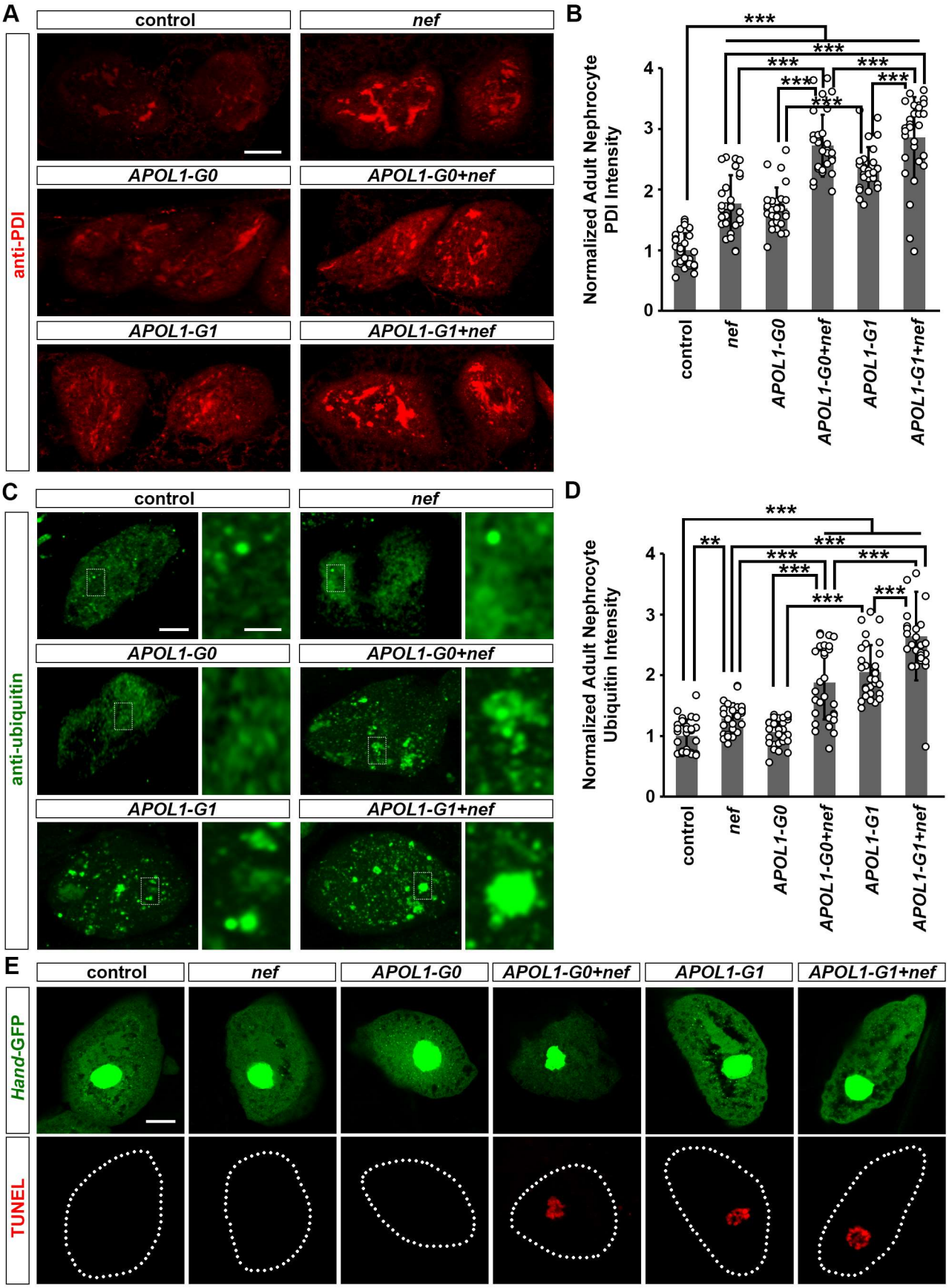
A
control
nef
APOL1-G0
APOL1-G0+nef
APOL1-G1
APOL1-G1+nef
anti-PDI
B
Normalized Adult Nephrocyte PDI Intensity
0
1
2
3
4
***
control
nef
APOL1-G0
APOL1-G0+nef
APOL1-G1
APOL1-G1+nef
C
control
nef
APOL1-G0
APOL1-G0+nef
APOL1-G1
APOL1-G1+nef
anti-ubiquitin
D
Normalized Adult Nephrocyte Ubiquitin Intensity
0
1
2
3
4
**
***
control
nef
APOL1-G0
APOL1-G0+nef
APOL1-G1
APOL1-G1+nef
E
control
nef
APOL1-G0
APOL1-G0+nef
APOL1-G1
APOL1-G1+nef
Hand-GFP
TUNEL

1070 **Figure 6. Model of HIV-1 Nef acting in synergy with APOL1-G1 through ER stress.**
1071 Graphic depiction of the proposed model by which HIV-1 Nef induces ER stress, which in turn
1072 leads to cellular toxicity. Via a separate pathway, Nef exacerbates APOL1-G1-mediated ER
1073 stress. APOL1-G1 disrupts the late endosomes and lysosomes, which affects the fusion of
1074 autophagosomes and lysosomes, the reduced autophagy results in protein accumulation,
1075 leading to ER stress. Thus, when together HIV-1 Nef and APOL1-G1 significantly increase
1076 cellular toxicity through ER stress, which ultimately leads to cell death and tissue damage in
1077 the kidneys. (Green text indicates data showed upregulation, whereas red text indicates data
1078 showed downregulation, yellow text indicates no change.) APOL1-G1, Apolipoprotein L1-risk
1079 allele G1; Atg8a-mCherry, Autophagy-related 8a with mCherry fluorescent tag; ER,
1080 endoplasmic reticulum; PDI, protein disulfide isomerase; Rab5/7-YFP, Rab5 or Rab7 with
1081 yellow fluorescent protein tag; Ref(2)p, refractory to sigma P; TUNEL, terminal
1082 deoxynucleotidyl transferase dUTP nick end labeling assay.
1083
1084
1085
1086
1087
1088
1089
1090
1091
1092
1093
1094
1095
1096
1097

Figure 6

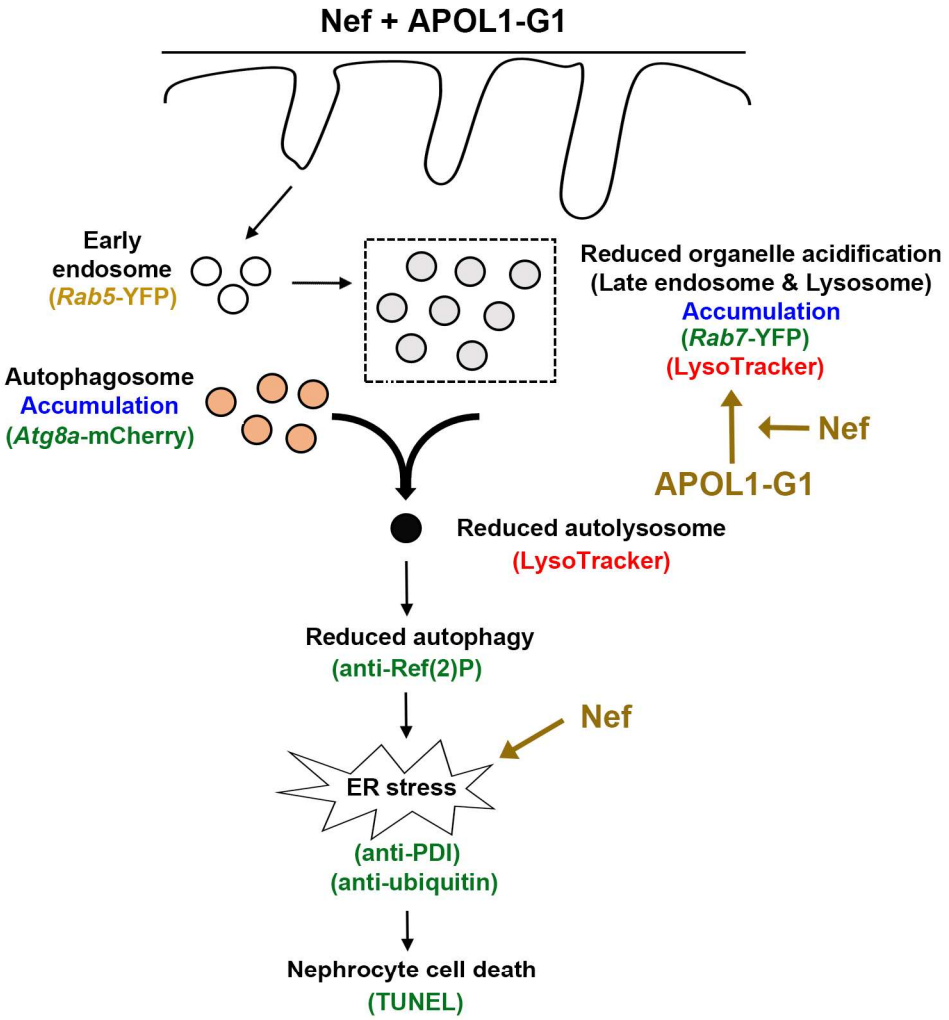
Nef + APOL1-G1
Early
endosome
(Rab5-YFP)
Reduced organelle acidification
(Late endosome & Lysosome)
Accumulation
(Rab7-YFP)
(LysoTracker)
Autophagosome
Accumulation
(Atg8a-mCherry)
Nef
APOL1-G1
Reduced autolysosome
(LysoTracker)
Reduced autophagy
(anti-Ref(2)P)
Nef
ER stress
(anti-PDI)
(anti-ubiquitin)
Nephrocyte cell death
(TUNEL)